

The evaluation of fish freshness by pressure testing

August 26, 1999

1 Introduction

A principal area of food research is the development of techniques for measuring the freshness of foodstuffs. For fish in particular, current standard tests rely heavily on “Sensory Evaluation Methods”, which involve scoring the smell, colour, appearance, taste, *etc.* of a fish sample. The scores are combined to a single “Quality Index” which is supposed to measure the freshness of the sample. There are many disadvantages to this approach, especially the expense involved in training people to conduct the tests and to rate different samples in an objective way.

Therefore the search is on for standardised tests of fish properties which could be used to evaluate freshness. Ideally, the tests should be

- **simple**, so that operators do not require expensive training;
- **robust**, so they can be used in the field rather than under controlled laboratory conditions;
- **fast**, preferably producing a reading within seconds or minutes rather than hours or days;
- **nondestructive**, so that stock need not be wasted on testing, and a customer can test fish for freshness before buying it.

These requirements rule out many possible techniques. For example, one can evaluate freshness very accurately by measuring microbe levels and/or protein degradation, but this requires at least twenty-four hours.

This document is concerned with a proposed new device for measuring the mechanical properties of a fish: it is believed that these may be correlated with freshness, at least for some species. The idea is to push a probe into the surface of the fish with some prescribed oscillatory motion, while the corresponding force is measured. This gives a measurement of the effective local mechanical properties of the flesh and has the advantages that (*i*) it can in principle be made reasonably small, such as for a hand-held device; (*ii*) if sufficiently small-amplitude oscillations are used, the sample need not be damaged; (*iii*) it should be feasible to obtain a reading within a few seconds.

A prototype experimental device has been built and tested at Robert Gordon University, and is described in section 2. The output from the device is time series for probe displacement

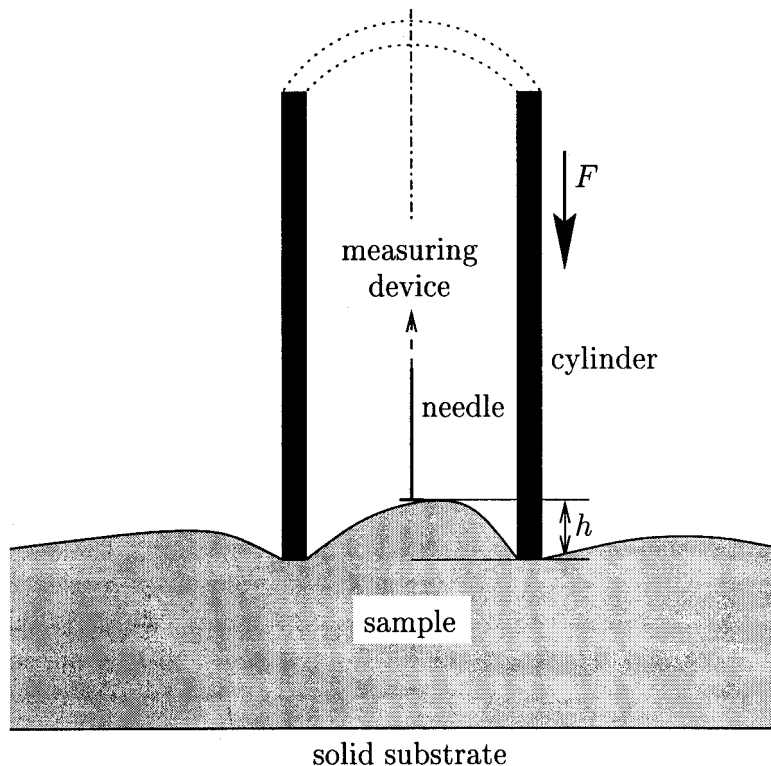


Figure 1: Schematic diagram of the experimental setup.

and force. Our first goal is to analyse these data mathematically. In section 2.1 we suggest a few simple quantities which can easily be determined from the time series and appear to be well correlated with the sample's mechanical properties.

In section 3 we present some possible mathematical modelling approaches to the problem. We begin by analysing a simple lumped-parameter viscoelastic model and comparing its predictions with the experimental observations. Next we improve on the model by allowing for loss of contact between the probe and the sample. We also discuss briefly the classical "punch" problem in which a probe is pushed into an elastic substrate. Finally we consider modelling the fish as a saturated deformable porous medium.

2 The experiment

The experimental setup is illustrated in figure 1. A cylinder is pushed into the surface of the sample to be tested and then oscillated up and down. The resulting force on the cylinder is measured versus time. To find the corresponding distance penetrated into the sample, a needle is suspended in the centre of the cylinder, and its displacement relative to the cylinder, which corresponds to the "meniscus height" h , is measured. Notice that h is *not* the same as the displacement relative to the equilibrium surface of the sample, but there is clearly a relation between the two. In practice, it is observed (though this has not yet been accurately measured) that *the top of the meniscus does not move very much as the probe is pushed in*, which implies that h can be identified with the relative displacement of the sample surface.

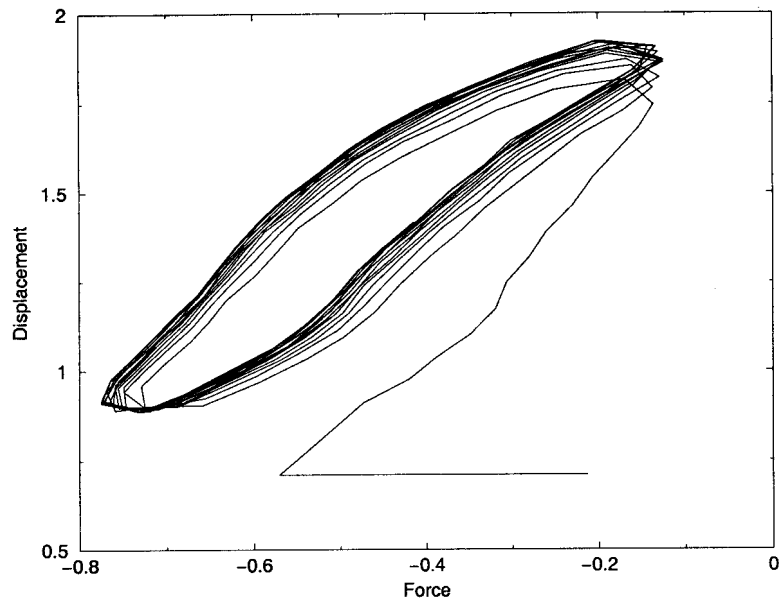


Figure 2: Meniscus height h versus force F (both uncalibrated) for a saturated sponge sample.

In the experiments performed at the Study Group the procedure adopted was as follows.

1. The cylinder is lowered until it appears to be in contact with the fish (see later discussion of contact). This maximum height is fixed thereafter.
2. Now the cylinder is lowered at constant speed (set by the operator) while the force F and meniscus height h are measured.
3. When F reaches a specified maximum value (also set by the operator) the motor is reversed and the cylinder is then raised at the same constant rate.
4. When the fixed maximum height is reached, the cycle repeats (*i.e.* we go back to step 2).

The description above makes it clear that a sawtooth displacement is imposed in the experiment. The period of the oscillations was typically several seconds. At the time of the Study Group the force and displacement measurements were not calibrated but were both given in terms of voltages. These were assumed to be related linearly to the actual values. However it is difficult to be certain exactly how much force was being applied and how deep the cylinder was penetrating in each experiment. As a rough guide we estimate that the displacements were typically a few millimeters in a sample a few centimetres deep. The inner and outer radii of the cylinder were 30mm and 40mm.

The above experiment was carried out on many different samples with different settings. In particular, we verified that linear displacement-force graphs were produced for materials we could expect to be reasonably linearly elastic (*e.g.* a credit card). For the purposes of this report we present the results only for three samples: a sponge saturated with water, a fresh

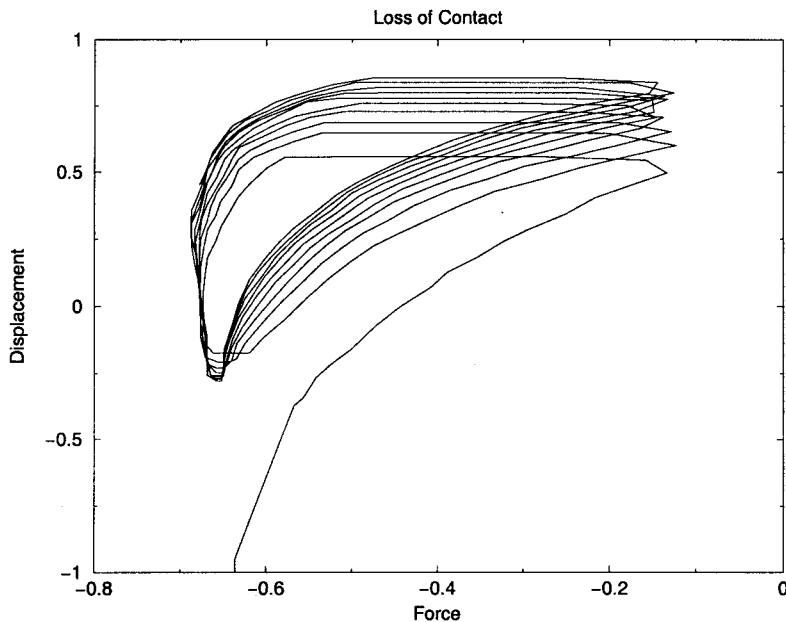


Figure 3: Meniscus height h versus force F (both uncalibrated) for a fresh fish sample with loss of contact.

fish and an old fish. In each case the settings on the apparatus were otherwise identical. The results are visualised by plotting h versus F as shown in figure 2 for the sponge. From this plot we make the following observations.

- After two or three cycles the system rapidly settles down to a robust periodic “limit cycle”, which is traversed in an anticlockwise sense.
- In both the loading and unloading parts of the cycle, the h versus F graph is curved, implying a nonlinear stress-strain relation for the sponge.
- The system is hysteretic, and the area enclosed inside the limit cycle corresponds to the energy lost during each period.

The last of these suggests a viscoelastic constitutive relation, but we should be cautious about jumping to such a conclusion. Qualitatively similar graphs were also generated by a *dry* sponge. However, prodding of the sponge suggested strongly that any viscoelastic relaxation times were *much* shorter (fractions of a second) than the timescale of the experiment, and thus that viscoelastic effects should be negligible. Therefore it may well be the case that the hysteresis seen in figure 2 is associated with specific properties of the sponge which make its responses during loading and unloading different, rather than any classical viscoelastic behaviour.

In figures 3 and 4 we show analogous graphs for samples of fresh fish and old fish respectively. We see that in either case, as for the sponge, a limit cycle is reached fairly rapidly. However, for both the fresh and the old fish samples, the cycle has a characteristic “banana” shape which is quite different from that seen in figure 2 for the sponge. At the high-force end the graphs become almost horizontal, implying that the fish becomes very stiff, while at

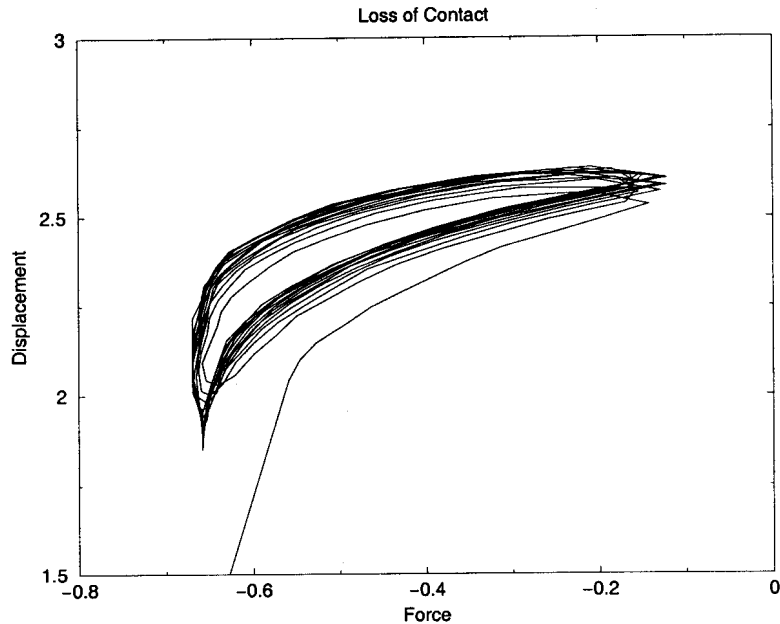


Figure 4: Meniscus height h versus force F (both uncalibrated) for an old fish sample with loss of contact.

the other end the graphs both have a vertical portion. This corresponds to loss of contact between the cylinder and the sample, and the uncalibrated force value (which appears to be around -0.67) corresponds to zero actual applied force. In both cases we can see that F actually drops *below* this value, implying that the force briefly becomes *negative*. This must result from adhesion between the surface of the fish and the cylinder as they lose contact.

This possibility of loss of contact between the sample and the cylinder seriously hinders the use of this experimental setup as a quantitative measurement system. Many of the features of experimental graphs like those shown in figures 2–4 (*e.g.* size and shape of limit cycle), which one might use to characterise the sample, depend crucially on the degree to which contact is lost. Moreover, we have seen that the cohesion between the sample and the cylinder can play an important role when contact is lost, and this is likely to be both difficult to characterise and highly sample-dependent.

Therefore it seems sensible to perform the experiments, and to design any future testing system based on them, in such a way that *contact between the sample and the cylinder is maintained at all times*. With the present setup we achieved this by starting the experiment with the cylinder already pushed a small distance into the sample. The resulting graph for a fresh fish sample is shown in figure 5. Now the banana shape is much less pronounced, with the very steep slope at small force eliminated. However, an undesirable feature is that the system appears to converge somewhat more slowly to the limit cycle. Moreover the limit cycle gradually drifts upwards as the apparatus damages the specimen.

It is not surprising that increasing the penetration to ensure good contact also increases the likelihood of sample damage, which is to be avoided since the test is intended to be non-destructive. Thus it appears that a compromise must be sought between (*i*) obtaining clean, reproducible results, and (*ii*) protecting the sample as much as possible.

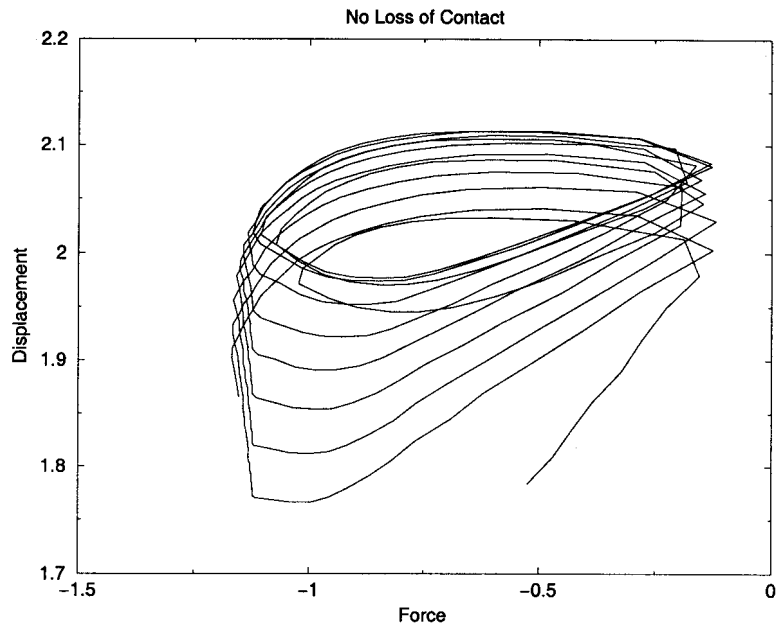


Figure 5: Meniscus height h versus force F (both uncalibrated) for a fresh fish sample without loss of contact.

2.1 Analysis of experimental results

In the graphs shown in figures 2–5, and others produced at the Study Group, we observe that the general *shape* of the limit cycle is obtained fairly closely within the first few cycles. However, it may continue to drift for several more cycles before settling down. Thus to obtain a stable repeatable reading we may have to run the test for some length of time, during which we run the danger of damaging the fish.

It seems sensible, therefore, to look for measurable properties which can quickly and easily be calculated from experimental data like those shown in figures 2–5, and which we hope could possibly be correlated with fish freshness. We propose to use

1. the *area* of the limit cycle which, as mentioned previously, corresponds to the energy loss;
2. the *principle moments* of the limit cycle, which characterise its shape (*e.g.* its eccentricity);
3. the *angle* made by the principle axis with the horizontal, which measures some averaged elastic modulus.

A simple program has been written which calculates these values as follows. First the area

$$A = \iint_{\text{cycle}} dF dh = \oint_{\text{period}} F dh, \quad (1)$$

where the line integral is readily approximated as a finite difference and thus obtained from experimental data points. Similarly it is easy to calculate the centroid and second moments

of the limit cycle via

$$A\bar{F} = \iint_{\text{cycle}} F dF dh = \oint_{\text{period}} \frac{F^2}{2} dh, \quad (2)$$

$$A\bar{h} = \iint_{\text{cycle}} h dF dh = \oint_{\text{period}} F h dh, \quad (3)$$

$$AM_{FF} = \iint_{\text{cycle}} F^2 dF dh = \oint_{\text{period}} \frac{F^3}{3} dh, \quad (4)$$

$$AM_{Fh} = \iint_{\text{cycle}} F h dF dh = \oint_{\text{period}} \frac{F^2 h}{2} dh, \quad (5)$$

$$AM_{hh} = \iint_{\text{cycle}} h^2 dF dh = \oint_{\text{period}} F h^2 dh. \quad (6)$$

Since we want to eliminate the drift of the limit cycle we subtract off the centroid (\bar{F}, \bar{h}) , defining

$$\tilde{M}_{FF} = \frac{1}{A} \iint_{\text{cycle}} (F - \bar{F})^2 dF dh = M_{FF} - \bar{F}^2, \quad (7)$$

$$\tilde{M}_{Fh} = \frac{1}{A} \iint_{\text{cycle}} (F - \bar{F})(h - \bar{h}) dF dh = M_{Fh} - \bar{F}\bar{h}, \quad (8)$$

$$\tilde{M}_{hh} = \frac{1}{A} \iint_{\text{cycle}} (h - \bar{h})^2 dF dh = M_{hh} - \bar{h}^2. \quad (9)$$

(Note that the centroid *can* readily be monitored also if desired; it might serve as a guide as to when sample damage is starting to occur and so the test should be halted.)

Now the principle moments are the eigenvalues of the tensor

$$\mathcal{M} = \begin{pmatrix} \tilde{M}_{FF} & \tilde{M}_{Fh} \\ \tilde{M}_{Fh} & \tilde{M}_{hh} \end{pmatrix},$$

that is

$$\lambda_{\pm} = \frac{1}{2} \left\{ \tilde{M}_{FF} + \tilde{M}_{hh} \pm \sqrt{(\tilde{M}_{FF} - \tilde{M}_{hh})^2 + 4\tilde{M}_{Fh}^2} \right\}, \quad (10)$$

and the angle made by the principle axis with the horizontal is given by

$$\tan \theta = \frac{\sqrt{(\tilde{M}_{FF} - \tilde{M}_{hh})^2 + 4\tilde{M}_{Fh}^2} + \tilde{M}_{hh} - \tilde{M}_{FF}}{2\tilde{M}_{Fh}}, \quad (11)$$

or

$$\theta = \frac{1}{2} \tan^{-1} \left(\frac{2\tilde{M}_{Fh}}{\tilde{M}_{FF} - \tilde{M}_{hh}} \right). \quad (12)$$

For each data point in the experiment we evaluated λ_+ , λ_- and θ over the preceding period. Their evolution over time is shown in figures 6–8 for the three samples analysed: the fresh fish with and without loss of contact, the old fish with loss of contact and the wet

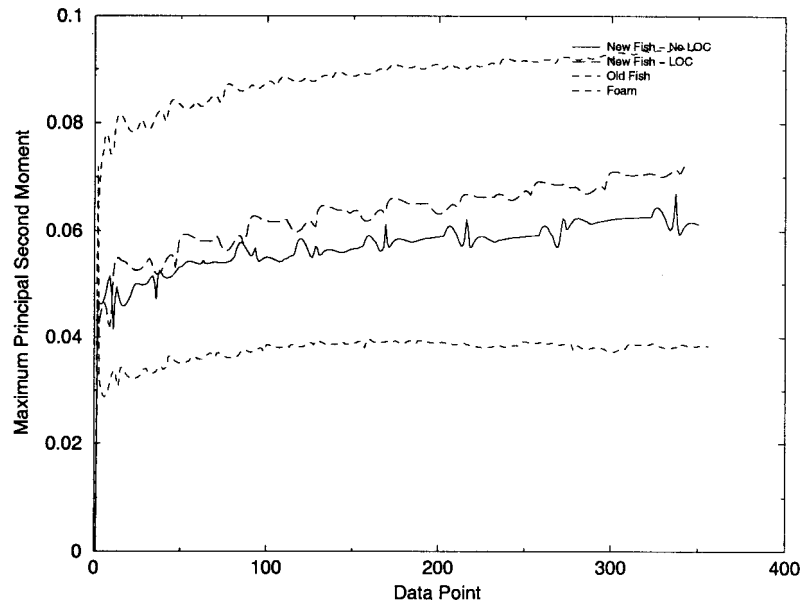


Figure 6: Maximum principal moment λ_+ versus time for (i) fresh fish without loss of contact, (ii) fresh fish with loss of contact, (iii) old fish with loss of contact, (iv) wet sponge with no loss of contact.

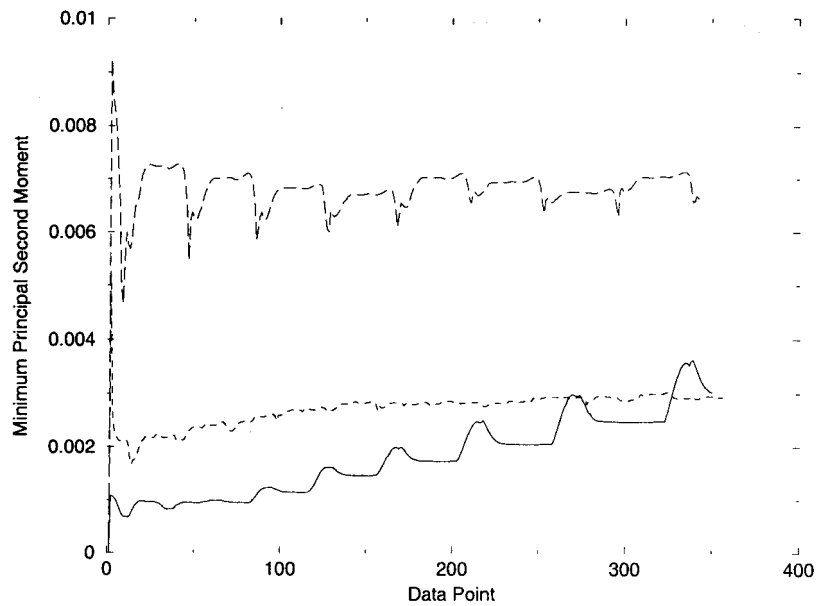


Figure 7: Minimum principal moment λ_- versus time for (i) fresh fish without loss of contact, (ii) fresh fish with loss of contact, (iii) old fish with loss of contact, (iv) wet sponge with no loss of contact.

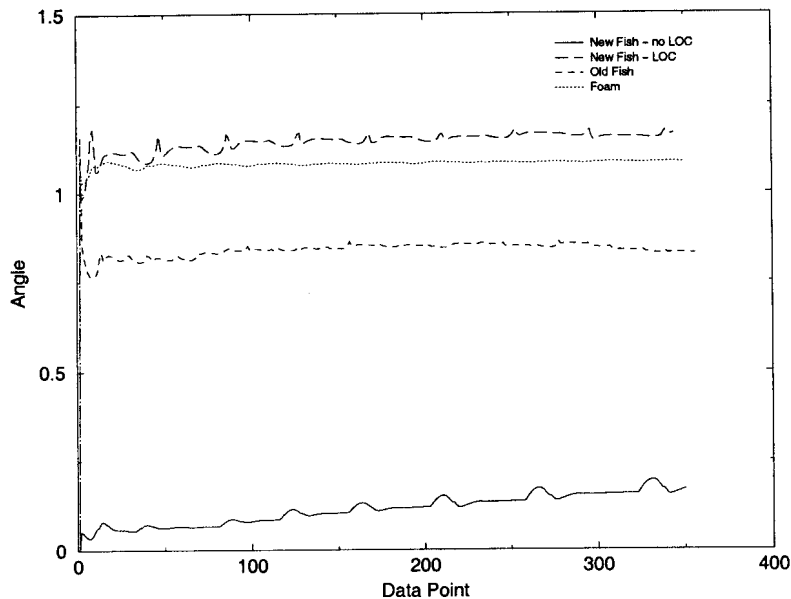


Figure 8: Angle θ made by the principle axis with the horizontal versus time for (i) fresh fish without loss of contact, (ii) fresh fish with loss of contact, (iii) old fish with loss of contact, (iv) wet sponge with no loss of contact.

sponge without loss of contact. The horizontal axis labels the data point at which each was evaluated; the time between data points was about 0.25 s in this experiment.

We should make the point that the old fish sample was considerably thinner than, and of a different species from, the fresh fish, so that no direct comparison between their measurements can safely be made. Nevertheless the graphs have some striking and encouraging features. In figures 6 and 8 we see that neither λ_+ nor θ varies dramatically during the experiment, implying that readings of these could be taken reasonably quickly. Moreover, the graphs for the fresh fish with and without loss of contact are grouped together, and markedly different from those for old fish and sponge. Thus λ_+ and θ do *not* appear to be too sensitive to the quality of contact, but can successfully distinguish between the three different samples.

In contrast, now consider figure 7. Here the readings *do* vary rather rapidly in places, making quick, repeatable measurement problematic, and continue to drift significantly. Also the contact problem appears to be much more of an issue for λ_- : the “old fish” graph lies between the two “fresh fish” curves. Thus it seems that λ_- is a somewhat less reliable indicator than either λ_+ or θ .

3 Mathematical models

Here we present a selection of mathematical modelling approaches each of which may be relevant to the mechanical testing of fish. We should note that in general the problem is extremely complex and we have not attempted to include all the possible physical complications in our models. A fish is a three-dimensional object comprised of muscle — a highly anisotropic, nonlinear viscoelastic material — supported by a flexible skeleton and saturated with water.

Compression of the fish results in deformation of the muscle and of the skeleton, and in the squeezing of water through the flesh. Moreover, as already mentioned there is the tricky issue of contact between the probe and the sample, which may depend on how “sticky” and/or “slippery” the surface of the fish is, and is further complicated by the fact that the fish may be encased in an elastic skin.

In this report we restrict our attention to very simple linear elastic and viscoelastic models, which cannot hope to capture all the detail described above. In our defence, we point out that any useful measuring device should *not* be too sensitive to such details, since we can expect large variations in size, shape and surface properties from one fish to another, as well as in where on the fish the measuring probe is placed. We can also argue that plastic deformations, although clearly significant in some of our experimental results (*e.g.* figure 5), should be ignored for the present, since the aim is to design a system which works without damaging the fish.

3.1 Lumped viscoelastic model

The simplest possible modelling approach is to attempt to describe the fish deformation by a single ordinary differential equation. If the behaviour is assumed to be linear and viscoelastic in nature, the most obvious choice is something of the form

$$a\dot{F} + bF = c\dot{v} + dv, \quad (13)$$

where v is the fish deformation, F is the applied force, a , b , c and d are nonnegative material parameters. Of course we could choose any one of these parameters to be unity, but it is safer for the moment to leave them all in so that each one in turn could be set to zero if desired. From the general form (13) the classical viscoelastic constitutive laws of Maxwell, Kelvin, *etc.* can be recovered by taking appropriate limits.

In the simplest configuration, where the probe always remains in contact with the sample, v is equal to the probe displacement h which, recall, is prescribed to be a sawtooth in time. We scale such that the displacement oscillates between 0 and 1 with period 2, as shown in figure 9. We note that *the analysis of this section would be considerably simpler if a sinusoidal forcing were employed*, as in more traditional rheometry.

Of course it is straightforward to write the general solution of (13) for $F(t)$ given $v(t)$:

$$F = \frac{1}{a} \int_0^t (c\dot{v} + dv) e^{b(\tau-t)/a} d\tau. \quad (14)$$

However, the sawtooth form of v makes direct work with this expression rather cumbersome, and one might as well solve (13) numerically. The result of such a calculation is shown in figure 10. We see that, as in the experimental graphs of figures 2–5, the solution settles down fairly rapidly to a limit cycle. This can readily be found analytically: the upper part of the cycle is given by

$$F = \frac{dh}{b} + \frac{bc - ad}{b^2(1 + e^{b/a})} \left(1 + e^{b/a} - 2e^{b(1-h)/a}\right), \quad (15)$$

and the lower by

$$F = \frac{dh}{b} - \frac{bc - ad}{b^2(1 + e^{b/a})} \left(1 + e^{b/a} - 2e^{bh/a}\right). \quad (16)$$

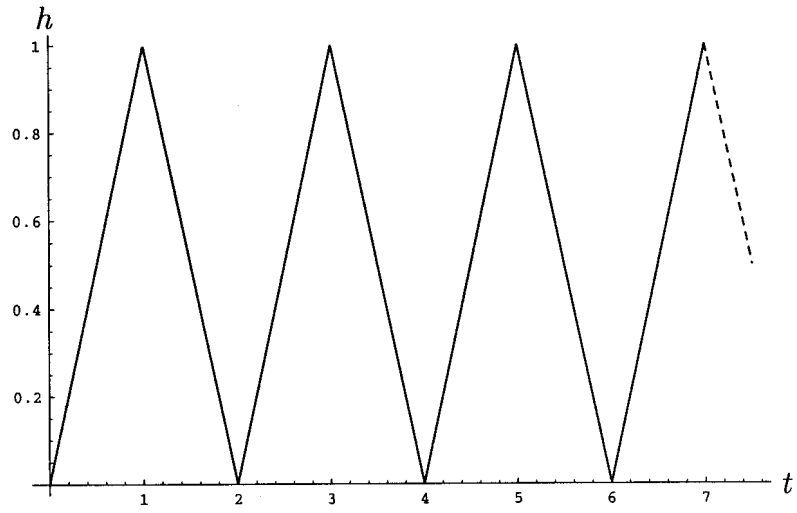


Figure 9: Prescribed “sawtooth” probe displacement.

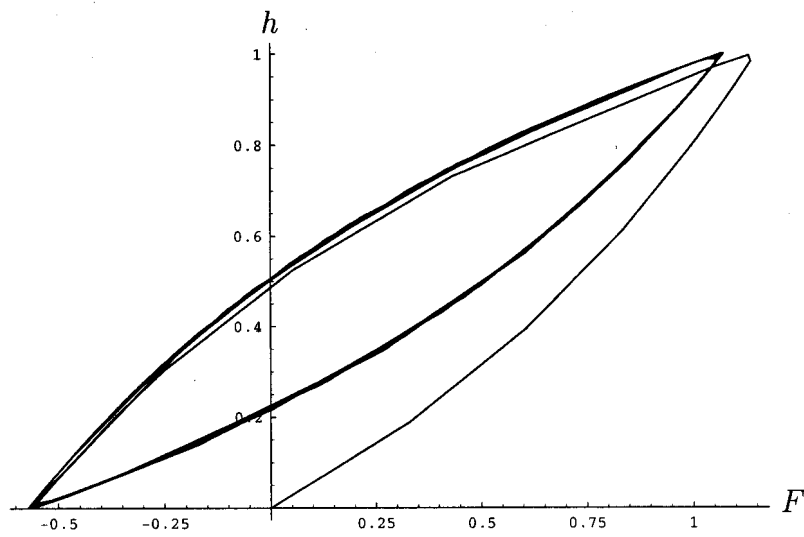


Figure 10: Numerical solution of the lumped o.d.e. (13) with parameter values $a = 0.5$, $b = 1$, $c = 1$, $d = 0.5$.

In particular, the minimum value taken by F during the cycle occurs at $h = 0$ and is

$$F_{\min} = \frac{ad - bc}{b^2} \tanh\left(\frac{b}{2a}\right), \quad (17)$$

so that F becomes negative if and only if $ad < bc$.

From the expressions (15, 16) we can readily calculate the area, moments, *etc.* defined in section 2.1:

$$A = \frac{2(bc - ad)(2a + b + (b - 2a)e^{b/a})}{b^3(1 + e^{b/a})}, \quad (18)$$

$$\bar{F} = \frac{d}{2b}, \quad \bar{h} = \frac{1}{2}, \quad (19)$$

and so forth. The lack of realism in the model as it stands (see below) means that it is not worthwhile to pursue the increasingly lengthy and complicated expressions for the higher-order moments.

Before modifying the model to make it more realistic, we note once more that the mathematical complication in analysing the solutions of (13) is almost entirely due to the sawtooth forcing function which is currently used. If this is replaced by the sinusoidal form

$$h(t) = \frac{1}{2} - \frac{1}{2} \cos(\pi t) = \sin^2\left(\frac{\pi t}{2}\right), \quad (20)$$

which represents the first two Fourier modes of the function shown in figure 9¹, the analysis becomes considerably more straightforward. We use the superscript ^s to denote the values obtained when h is given by (20). In this case one can readily solve (13) as an initial-value problem for $F(t)$ (assuming $F(0) = 0$):

$$F^s = \frac{d}{2b} + \frac{(bc - ad)\pi \sin(\pi t) - (bd + ac\pi^2) \cos(\pi t)}{2(b^2 + a^2\pi^2)} + \frac{a(bc - ad)\pi^2 e^{-bt/a}}{2b(b^2 + a^2\pi^2)}, \quad (21)$$

where the first two terms clearly represent the limit cycle. The area, centroid and moments of this limit cycle are also much easier to obtain than for the sawtooth forcing:

$$A^s = \frac{(bc - ad)\pi^2}{4(b^2 + a^2\pi^2)}, \quad \bar{F}^s = \frac{d}{2b}, \quad \bar{h}^s = \frac{1}{2}, \quad (22)$$

$$\bar{M}_{FF}^s = \frac{d^2 + c^2\pi^2}{16(b^2 + a^2\pi^2)}, \quad \bar{M}_{Fh}^s = \frac{bd + ac\pi^2}{16(b^2 + a^2\pi^2)}, \quad \bar{M}_{hh}^s = \frac{1}{16}. \quad (23)$$

In general, for sinusoidal forcing of the form

$$h = \bar{h} + \epsilon e^{i\omega t}$$

(real part assumed) we can look for periodic solutions

$$F = \bar{F} + G\epsilon e^{i\omega t}, \quad \bar{F} = d\bar{h}/b.$$

¹Of course one way to solve (13) is to expand $h(t)$ as an infinite Fourier series. This however introduces its own problems through Gibbs' phenomenon when h is not smooth.

Thus the centroid is determined by the elastic modulus d/b , while for given ω the shape of the limit cycle is given in terms of the *complex modulus* $G(\omega)$:

$$A = \pi|\epsilon|^2\Im(G), \quad \bar{M}_{FF} = \frac{|\epsilon|^2|G|^2}{4}, \quad \bar{M}_{Fh} = \frac{|\epsilon|^2\Re(G)}{4}, \quad \bar{M}_{hh} = \frac{|\epsilon|^2}{4}. \quad (24)$$

For the constitutive relation (13) G is simply given by

$$G = \frac{d + i\omega c}{b + i\omega a}. \quad (25)$$

Thus for a single frequency ω , by measuring the position and shape of the limit cycle we obtain d/b , and the real and imaginary parts of G . This gives us three relations which determine the constants a, b, c, d up to an arbitrary scaling, except for the critical case $ad = bc$ in which the limit cycle collapses onto a line segment.

For more general constitutive relations than (13), so long as they are linear we can still define G in the same way and relate it to the limit cycle shape by (24). Again, for each ω we can only obtain three pieces of information from the properties of the limit cycle. Therefore, if the material is characterised by more than three parameters, we must vary ω , and try to determine the constitutive relation by monitoring the variations of $\Re(G)$ and $\Im(G)$ with ω .

3.2 Loss of contact

The limit cycle defined by (15, 16) or by (20, 21) is always (i) convex and (ii) symmetric, neither of which is always the case for experimental curves (see in particular figures 3 and 4). Moreover, figure 10 shows that the force F may become negative at small h , which implies suction of the probe by the sample; as discussed above this occurs if and only if $ad < bc$. This is unrealistic; while as noted in section 2 there *may* be a small amount of adhesion as the probe loses contact with the fish, it is certainly not of the magnitude of that shown in figure 10, and in any case is not described by the model (13).

To address some of these issues, we now consider a simple model for an experiment in which the probe may lose contact with the sample. First, suppose the probe is in contact with the sample, so we have $v = h$. We require the force F to be positive; when F reaches zero we suppose the probe loses contact with the sample and subsequently we require $v > h$ while $F = 0$. This continues until v catches up with h when we return to the contact scenario. Thus the problem to be solved is the o.d.e. (13) with

$$\begin{aligned} &\text{either (i) contact} \Rightarrow v = h, F > 0, \\ &\text{or (ii) no contact} \Rightarrow v > h, F = 0. \end{aligned} \quad (26)$$

As before, this can be solved numerically, and the limit cycle can be found analytically, at least up to the solution of a couple of transcendental equations. The cycle starts with no contact until h reaches a critical value h_{c1} at which contact occurs:

$$F = 0, \quad 0 < h < h_{c1}, \quad (27)$$

$$F = \frac{bc - ad}{b^2} \left(1 - e^{b(h_{c1}-h)/a}\right) + \frac{d}{b} \left(h - h_{c1} e^{b(h_{c1}-h)/a}\right), \quad h_{c1} < h < 1. \quad (28)$$

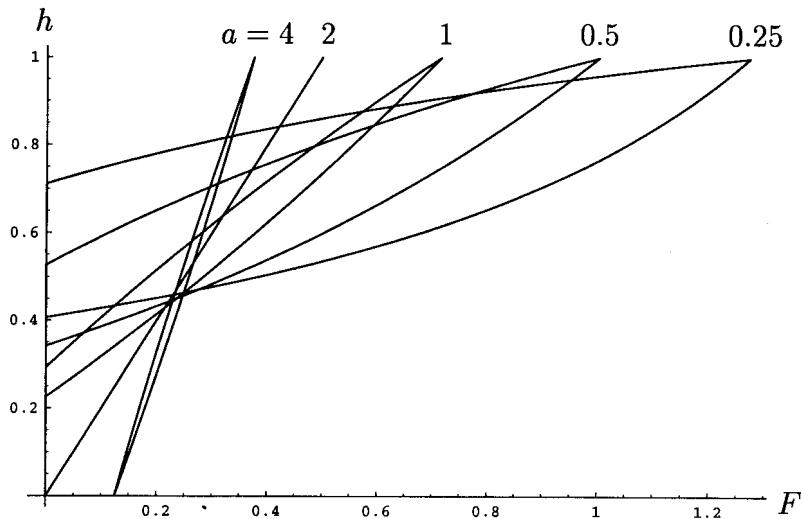


Figure 11: Probe height h versus force F for the lumped parameter model with loss of contact. The parameter values are $b = 1$, $c = 1$, $d = 0.5$ and $a = 0.25, 0.5, 1, 2, 4$.

Then, as h is decreased from 1, the probe remains in contact until a second critical value $h_{c2} > h_{c1}$ is reached, at which contact is lost once more:

$$F = \frac{bc - ad}{b^2} \left(e^{b(h-h_{c2})/a} - 1 \right) + \frac{d}{b} \left(h - h_{c2} e^{b(h-h_{c2})/a} \right), \quad 1 > h > h_{c2}, \quad (29)$$

$$F = 0, \quad h_{c2} > h > 0. \quad (30)$$

The values of h_{c1} and h_{c2} are determined by the system

$$(bc - ad) \left(1 - 2e^{b(h_{c2}-1)/a} + e^{b(h_{c1}+h_{c2}-2)/a} \right) = bd \left(h_{c2} - h_{c1} e^{b(h_{c1}+h_{c2}-2)/a} \right), \quad (31)$$

$$h_{c2} = h_{c1} e^{d(h_{c1}+h_{c2})/c}. \quad (32)$$

In figure 11 we show the form of this limit cycle for $b = 1$, $c = 1$, $d = 0.5$ and various values of a . For $a = 4$ we have $ad > bc$ so there is no loss of contact; $a = 2$ is the critical value at which the limit cycle collapses onto a line segment; when $a = 1$ we first observe loss of contact with the vertical segment of the cycle in which $F = 0$; as a is decreased further the cycle grows and flattens, and the region of loss of contact grows likewise. On the whole, the introduction of contact loss into the model has made the graphs more like the “banana” shapes shown in figures 3 and 4. However, it still does not capture the concavity of the lower part of the cycle; we speculate that this arises from nonlinear effects which cannot be described by (13).

3.3 Elastic punch models

The problem of finding the stresses and displacements caused by the indentation of an elastic half-space by a punch is a classical problem in linear elasticity. Here we quote the results of Spence 1968 for the case of a flat-ended cylindrical punch, which seems most relevant to the present problem. The solution depends on whether the punch is *smooth*, so that the substrate can slip freely under it, or *rough*, in which case there is no slip between punch and substrate.

In either case, a relation is obtained between the inward punch displacement h and the applied force F :

$$\text{smooth punch} \Rightarrow F = \frac{2Eah}{1-\nu^2}, \quad (33)$$

$$\text{rough punch} \Rightarrow F = \frac{2Eah \log(3-4\nu)}{(1-\nu)(1-2\nu)}, \quad (34)$$

where a is the radius of the punch, and E and ν are the Young's modulus and Poisson ratio of the substrate.

Note that similar results can be obtained for the corresponding two-dimensional indentation problem (see *e.g.* England 1971). Indeed it may be that a two-dimensional geometry is applicable to the annular probe described in section 2. As noted there it is observed that the centre of the meniscus appears to remain fixed as the probe is pressed into the sample. This suggests that the annulus is wide enough that the opposite sides do not influence each other much, and hence that a two-dimensional approach should serve as a reasonable first approximation.

The results (33, 34) could be made more realistic in many other ways, for example by making the substrate finite, considering different punch shapes or allowing more general contact conditions. It is unlikely that analytical solutions will be available in these cases, although they could of course be tackled numerically. However, it is clear that so long as linear elasticity is employed, the *form* of the force-displacement law must be similar to (33, 34), namely

$$F = Eahf,$$

where f is a dimensionless function of ν and the geometry of the substrate and punch.

Equally, even if a linear viscoelastic law is employed, for sinusoidal motion of the punch the force-displacement law must still take a similar linear form:

$$F = Gh,$$

where as before G is the effective complex modulus, which will depend on the geometry under consideration as well as the material parameters of the substrate.

Finally we note in passing that solutions can also be found for the penetration of *plastic* bodies (see Calladine 1985). We will not dwell on this for the reason quoted above, that the aim is to avoid testing procedures which damage the sample.

3.4 Deformable porous medium model

It is believed that the squeezing of water through the fish flesh as the fish is compressed by the probe gives rise to an important component of the force which is measured and helps to explain the hysteresis which is observed. Therefore we now consider modelling the fish as a deformable porous medium (Biot 1955).

The picture is of an elastic solid matrix which is saturated with water. We denote the velocities of the solid and liquid phases by \mathbf{u}_s and \mathbf{u}_l respectively and the volume fraction of liquid by α . Since we assume that the matrix is everywhere saturated, the solid fraction is

simply $1 - \alpha$ and we need not concern ourselves with infiltration, wetting fronts and so forth (e.g. Sommer & Mortensen 1996). Thus, if we assume that both phases are incompressible, conservation of mass for each phase reads

$$\alpha_t + \nabla \cdot [\alpha \mathbf{u}_l] = 0, \quad (35)$$

$$-\alpha_t + \nabla \cdot [(1 - \alpha) \mathbf{u}_s] = 0. \quad (36)$$

The relative velocity between the two phases is assumed to satisfy Darcy's law

$$\mathbf{u}_l - \mathbf{u}_s = -\frac{1}{\eta} \mathbf{K}(\alpha) \cdot \nabla p, \quad (37)$$

where p is the liquid pressure, η the shear viscosity and \mathbf{K} the permeability tensor. Here we will only consider the isotropic case in which \mathbf{K} can be replaced by a scalar k , which is nevertheless usually strongly dependent on α .

Finally, a balance of total stress (neglecting inertia and gravity) gives

$$\nabla p = \nabla \cdot \boldsymbol{\sigma}, \quad (38)$$

where $\boldsymbol{\sigma}$ is the *effective stress tensor* in the solid matrix. This is defined to be the stress acting in the solid, averaged over a surface area comprising both liquid and solid. Thus $\sigma_{ij} - p\delta_{ij}$ is the total stress in the fully saturated porous material. Put another way, $\boldsymbol{\sigma}$ is the stress tensor that one would measure in a completely dry sponge; p accounts for the extra component due to the presence of water. Once a constitutive relation has been proposed for $\boldsymbol{\sigma}$ (as well as a functional form for $k(\alpha)$) (35–38) gives a closed system for α , \mathbf{u}_l , \mathbf{u}_s and p .

3.4.1 One-dimensional model

As a first simple example, consider a purely one-dimensional problem, with

$$\mathbf{u}_l = \begin{pmatrix} 0 \\ 0 \\ w_l \end{pmatrix}, \quad \mathbf{u}_s = \begin{pmatrix} 0 \\ 0 \\ w_s \end{pmatrix}, \quad \boldsymbol{\sigma} = \begin{pmatrix} 0 & 0 & 0 \\ 0 & 0 & 0 \\ 0 & 0 & \sigma \end{pmatrix},$$

and everything dependent on just one spatial component z and time t . Then (35–38) reduces to

$$\alpha_t + [\alpha w_l]_z = 0, \quad (39)$$

$$-\alpha_t + [(1 - \alpha)w_s]_z = 0, \quad (40)$$

$$w_l - w_s = -\frac{k}{\eta} p_z, \quad (41)$$

$$p_z = \sigma_z. \quad (42)$$

For purely one-dimensional motion, the specification of a constitutive relation for $\boldsymbol{\sigma}$ is particularly simple: we need only specify a relation between σ and the liquid fraction α . Typically $\sigma(\alpha)$ should be monotonic increasing in α , with $\sigma \rightarrow -\infty$ as $\alpha \rightarrow 0$ and $\sigma \rightarrow \infty$ as $\alpha \rightarrow 1$. The equilibrium state is thus defined by the zero of $\sigma(\alpha)$, say $\sigma(\alpha_0) = 0$.

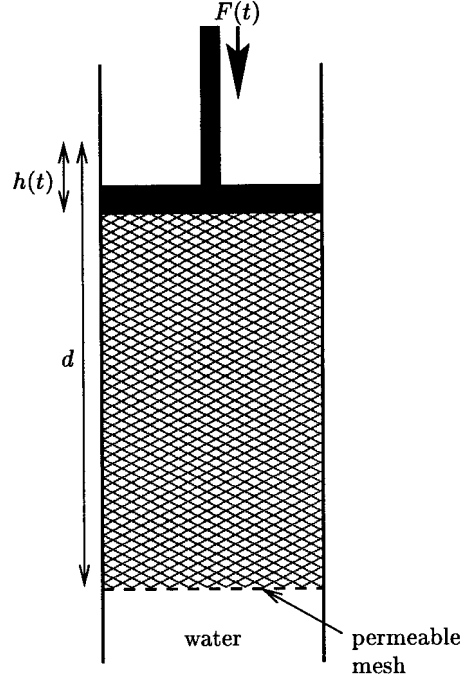


Figure 12: Schematic of a one-dimensional squeezing experiment.

Now by adding (39) to (40) and integrating we obtain

$$\alpha w_l + (1 - \alpha)w_s = q(t) \quad \Rightarrow \quad w_s = -\frac{\alpha w_l}{1 - \alpha} + \frac{q}{1 - \alpha}, \quad (43)$$

where q represents the total flux of solid and liquid and is given by the boundary conditions. Then by combining this with (41) and (42) we find

$$w_l = q - \frac{k}{\eta}(1 - \alpha)\sigma'(\alpha)\alpha_z. \quad (44)$$

Finally, by substituting this expression for w_l into (39) we obtain a convection-diffusion equation for α :

$$\alpha_t + q\alpha_z = \frac{1}{\eta} [(1 - \alpha)k(\alpha)\sigma'(\alpha)\alpha_z]_z. \quad (45)$$

In suggesting suitable boundary conditions for (45) we consider the experimental scenario shown schematically in figure 12. Here a layer of saturated porous material with initial height d sits on a porous base over a reservoir of water. A plunger is pushed a distance $h(t)$ into the top of the layer and the corresponding force $F(t)$ is measured.

At the top of the layer both the liquid and solid velocities must equal that of the plunger,

$$w_l = w_s = -\dot{h} \quad \text{on } z = d - h(t),$$

and therefore

$$q(t) \equiv -\dot{h}, \quad (46)$$

and

$$\alpha_z = 0 \quad \text{on } z = d - h(t). \quad (47)$$

At the bottom $z = 0$ the solid velocity w_s is zero and thus

$$\alpha k(\alpha) \sigma'(\alpha) \alpha_z = \eta \dot{h} \quad \text{on } z = 0. \quad (48)$$

Given $h(t)$, the boundary conditions (47, 48), along with the initial condition

$$\alpha = \alpha_0 \quad \text{at } t = 0, \quad (49)$$

are sufficient to solve (45). Next we determine the force F (per unit area in the $\{x, y\}$ plane) applied to the plunger. From (42) we have

$$F(t) = p - \sigma.$$

Since the boundary $z = 0$ is assumed to be permeable p is zero there, and so F is simply given by

$$F(t) = -\sigma(\alpha(0, t)). \quad (50)$$

Before looking for solutions of this problem we first obtain a relation representing total conservation of the solid phase by integrating (40) with respect to z and applying the boundary conditions on $z = 0$ and $z = d - h$:

$$\int_0^{d-h} (1 - \alpha) dz = \text{const.} = (1 - \alpha_0)d. \quad (51)$$

Now we start by looking for a steady solution of (45–48) with $h = \bar{h} = \text{const.}$ Thus $q = 0$ and (45) implies that $\alpha_z = \text{const.}$ The boundary condition (47) tells us that this constant is zero, *i.e.* that α is constant, say $\bar{\alpha}$. Then (51) gives

$$\bar{\alpha} = \frac{\alpha_0 d - \bar{h}}{d - \bar{h}}. \quad (52)$$

Note that we require $\bar{h} < \alpha_0 d$ so that $\bar{\alpha}$ is positive. Finally, (50) gives the force

$$\bar{F} = -\sigma(\bar{\alpha}). \quad (53)$$

Thus, as might have been anticipated, in the steady state, the stress is purely elastic. Note that $\bar{\alpha}$ is a decreasing function of \bar{h} while σ is an increasing function of α so that \bar{F} increases with \bar{h} , as expected.

Now consider an oscillatory perturbation, with

$$h = \bar{h} + \epsilon e^{i\omega t}, \quad F = \bar{F} + G\epsilon e^{i\omega t}, \quad \alpha = \bar{\alpha} + \epsilon f(z) e^{i\omega t}. \quad (54)$$

After linearising with respect to ϵ we obtain

$$Df''(z) = i\omega f(z), \quad D = \frac{(1 - \bar{\alpha})k(\bar{\alpha})\sigma'(\bar{\alpha})}{\eta}, \quad (55)$$

with boundary conditions

$$f'(d - \bar{h}) = 0, \quad \frac{\bar{\alpha}}{1 - \bar{\alpha}} D f'(0) = i\omega, \quad (56)$$

and the solution is

$$f = -\frac{1 - \bar{\alpha}}{\bar{\alpha}} \sqrt{\frac{i\omega}{D}} \frac{\cosh\left(\frac{(z - d + \bar{h})\sqrt{i\omega/D}}{D}\right)}{\sinh\left(\frac{(d - \bar{h})\sqrt{i\omega/D}}{D}\right)}. \quad (57)$$

Then (50) gives the complex modulus

$$G = \frac{F}{h} = -\sigma'(\bar{\alpha})f(0) = \frac{(1 - \bar{\alpha})\sigma'(\bar{\alpha})}{\bar{\alpha}} \sqrt{\frac{i\omega}{D}} \coth\left(\sqrt{\frac{i\omega}{D}}(d - \bar{h})\right). \quad (58)$$

The expressions (53, 58) for \bar{F} and G can be related to the position and shape of a measured limit cycle exactly as in section 2.1. Thus information about $\sigma(\alpha)$ and $k(\alpha)$ can be obtained, and these material properties of the flesh may hopefully be correlated with freshness.

3.4.2 Linear elastic model

As soon as we abandon the one-dimensional configuration considered above, there are serious difficulties involved in constituting the elastic stress tensor σ . If, as in section 3.4.1, we allow α to change by a finite amount, to be consistent we must also employ fully nonlinear elasticity in our model for σ . While in one dimension this merely involves specifying a single scalar function $\sigma(\alpha)$, in three dimensions the general equations are gruesome.

To avoid such complications, we henceforth consider only infinitesimal changes in α , which corresponds to assuming that h is infinitesimal, so that σ can be described using linear elasticity. To this end we define a displacement field \mathbf{U} in the solid matrix; within the linear theory, this is related to the velocity \mathbf{u}_s by

$$\frac{\partial \mathbf{U}}{\partial t} = \mathbf{u}_s. \quad (59)$$

Then we propose the usual linear elastic constitutive relation for σ :

$$\sigma_{ij} = \lambda \frac{\partial U_k}{\partial x_k} \delta_{ij} + \mu \left(\frac{\partial U_i}{\partial x_j} + \frac{\partial U_j}{\partial x_i} \right), \quad (60)$$

where λ and μ are the Lamé constants. Recall that this constitutive relation is for the *matrix as a whole*, not for the elastic material of which it is made.

As noted above, our use of linear elasticity assumes that the velocities \mathbf{u}_l , \mathbf{u}_s are small and that α varies by a small amount. Thus we set

$$\alpha = \alpha_0 + \tilde{\alpha}, \quad (61)$$

and linearise (35–38) with respect to $\tilde{\alpha}$, p , \mathbf{u}_s and \mathbf{u}_l . Of these, (36) reduces to

$$-\tilde{\alpha}_t + (1 - \alpha_0) \nabla \cdot \mathbf{u}_s = 0,$$

which, after substitution for \mathbf{u}_s from (59), can be integrated with respect to t to give

$$\nabla \cdot \mathbf{U} = \frac{\tilde{\alpha}}{1 - \alpha_0}. \quad (62)$$

Conservation of liquid (35) implies

$$\tilde{\alpha}_t + \alpha_0 \nabla \cdot \mathbf{u}_l = 0, \quad (63)$$

while Darcy's law and conservation of momentum (41, 42) combine to

$$\mathbf{U}_t - \mathbf{u}_l = \frac{k(\alpha_0)}{\eta} \nabla p = \frac{k(\alpha_0)}{\eta} \nabla \cdot \boldsymbol{\sigma}. \quad (64)$$

With $\boldsymbol{\sigma}$ defined by (60), (62–64) form a closed system for $\tilde{\alpha}$, p , \mathbf{U} and \mathbf{u}_l .

We deduce a single equation for $\tilde{\alpha}$ by taking the divergence of (64), substituting for \mathbf{U} and \mathbf{u}_s from (62, 63) and noting that

$$\nabla \cdot (\nabla \cdot \boldsymbol{\sigma}) = (\lambda + 2\mu) \nabla^2 (\nabla \cdot \mathbf{U}).$$

Thus we find that $\tilde{\alpha}$ satisfies the heat equation

$$\tilde{\alpha}_t = D \nabla^2 \tilde{\alpha}, \quad D = \frac{\alpha_0 k(\alpha_0) (\lambda + 2\mu)}{\eta}. \quad (65)$$

This looks deceptively simple: in general the boundary conditions will not be easily stated in terms of $\tilde{\alpha}$, and a more useful rearrangement of the equations is

$$\nabla^2 p = \frac{\eta}{\alpha_0 k(\alpha_0)} \nabla \cdot \mathbf{U}_t, \quad (66)$$

$$\nabla p = (\lambda + \mu) \nabla (\nabla \cdot \mathbf{U}) + \mu \nabla^2 \mathbf{U}. \quad (67)$$

To fix ideas, consider the two-dimensional scenario shown in figure 13 (of course we could equally consider a radially-symmetric version, with x replaced by r). Here a sponge with initial length l and height d , is immersed in a bath of water. A probe of thickness $2a$ is pushed a distance $h(t)$ into the top of the sponge. Only half the geometry is shown; symmetry about the x -axis is assumed. We now examine what boundary conditions might be appropriate in modelling such an experiment. Since the problem is two-dimensional, we set $\mathbf{U} = (U, W)$.

The base $z = 0$ is assumed to be impermeable, which implies $p_z = 0$. For the displacement \mathbf{U} , we must decide whether the sponge is stuck to the base or free to slip; in the former case we have $\mathbf{U} = 0$, while in the latter, the normal displacement W , and the tangential stress σ_{xz} are zero, that is

$$\text{no slip} \Rightarrow p_z = U = W = 0 \quad \text{on } z = 0, \quad (68)$$

$$\text{free slip} \Rightarrow p_z = U_z = W = 0 \quad \text{on } z = 0. \quad (69)$$

In general we could impose a friction law which contains both (68) and (69) as limits, but this is unnecessarily complicated for our purposes. For a real fish, which is attached to a rigid skeleton down its middle, (68) is probably the more physically relevant.

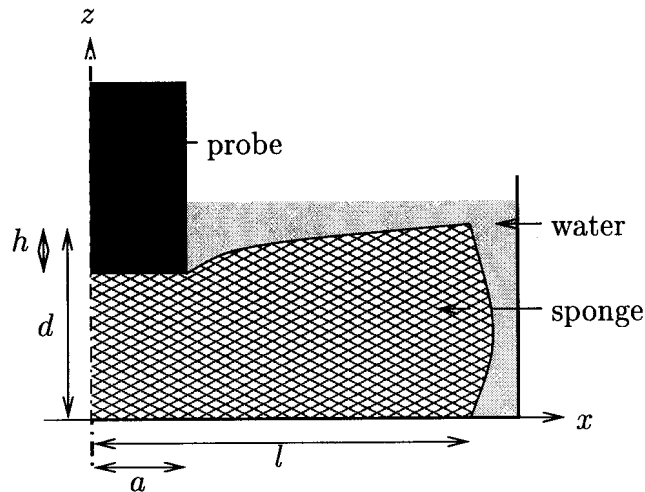


Figure 13: Schematic of a two-dimensional squeezing experiment.

Similar considerations apply below the probe. Once again impermeability implies a Neumann condition for p . Now the normal displacement of the solid phase must be equal to that of the probe, and for the tangential component as before we can impose zero slip or free slip:

$$\text{no slip} \Rightarrow p_z = U = 0, W = -h \quad \text{on } z = d, \quad (70)$$

$$\text{free slip} \Rightarrow p_z = U_z = 0, W = -h \quad \text{on } z = d. \quad (71)$$

Notice that the boundary conditions are imposed on the *undeformed* surface by linearisation.

The side $x = l$ of the sponge is assumed to be fully permeable so that the pressure satisfies Dirichlet data, and stress-free *i.e.* $\sigma_{xx} = \sigma_{xz} = 0$, and thus

$$p = U_z + W_x = (\lambda + 2\mu)U_x + \lambda W_z = 0 \quad \text{on } x = l. \quad (72)$$

If the top free surface is also assumed to be perfectly permeable then boundary conditions analogous to (72) should be applied there. However, we might also want to consider cases where the top surface is *impermeable*, *e.g.* for a fish sample with a skin. In the latter case we have a Neumann condition for p and zero *total* stress:

$$\text{permeable} \Rightarrow p = U_z + W_x = \lambda U_x + (\lambda + 2\mu)W_z = 0 \quad \text{on } z = d, x > a, \quad (73)$$

$$\text{impermeable} \Rightarrow p_z = U_z + W_x = \lambda U_x + (\lambda + 2\mu)W_z - p = 0 \quad \text{on } z = d, x > a. \quad (74)$$

As with the slip conditions imposed above, one could use a combination of (73) and (74) to model a semi-permeable surface.

Finally, we impose the usual symmetry conditions on the centre-line

$$p_x = U = W_x = 0 \quad \text{on } x = 0, \quad (75)$$

and initial condition

$$U = W = 0 \quad \text{at } t = 0. \quad (76)$$

With $h(t)$ specified (and assuming $h(0) = 0$), the boundary conditions (68 or 69, 70 or 71, 72, 73 or 74, 75) and initial conditions (76) are sufficient to solve the system (66, 67)

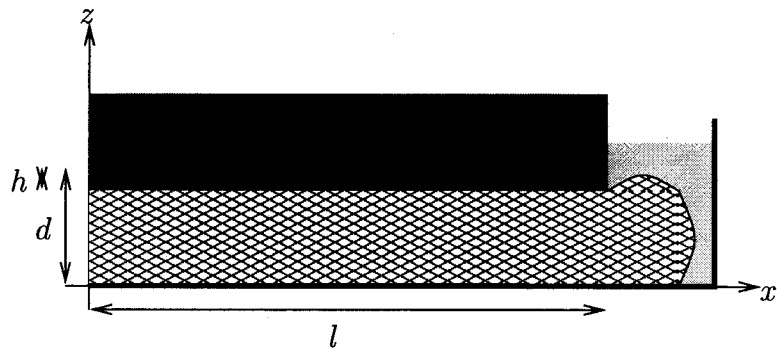


Figure 14: Schematic of a *slender* two-dimensional squeezing experiment.

numerically. We do not attempt such a solution in this report, but note that it should be reasonably straightforward with the aid of a package such as *fastflo*. The desired output from such a calculation is the force (per unit length in the third dimension) exerted on the probe, which is given by

$$F = 2 \int_0^a [p - \lambda U_x - (\lambda + 2\mu)W_z]_{z=d} dx. \quad (77)$$

3.4.3 Lateral squeezing model

A weakness of the one-dimensional model described in section 3.4.1 is that we cannot make the base $z = 0$ impermeable without running into a contradiction unless $\dot{h} = 0$. This is because we have not allowed for lateral squeezing of the liquid as the probe is pushed in, although in the sponge experiments this lateral motion of the water was observed to be significant. Of course such effects are fully accounted for (albeit for small deformations) by the theory of section 3.4.2, but this requires numerical solution rather than furnishing a simple expression like (58) for the complex modulus which can easily be compared with experiments.

Therefore we now propose a quasi-one-dimensional model which includes lateral squeezing but is considerably simpler than the two-dimensional theory of section 3.4.2. The model is obtained under the assumption that the geometry is slender in the x -direction, that is $d \ll l$ as shown in figure 14. We emphasise that this is not intended to be representative of the real experimental configuration: the purpose of considering this limit is to obtain a simple “lumped parameter” model like (58) which improves on the one-dimensional theory by including lateral motion.

Under the usual assumptions of lubrication theory (essentially that z -derivatives dominate over x -derivatives), the two-dimensional system (66, 67) can be simplified to

$$(U_x + W_z)_t = D(U_x + W_z)_{zz}, \quad (78)$$

$$p_x = \mu U_{zz}, \quad (79)$$

$$p_z = 0, \quad (80)$$

with D as in (65).² For simplicity we consider only the no-slip boundary conditions $U = 0$

²We present all the equations in dimensional form and take the “lubrication” limit in an heuristic manner; however, we point out that the analysis could be made more systematic by nondimensionalising and using asymptotic expansions.

on $z = 0, d$, and hence

$$U = \frac{p_x}{2\mu} z(z - d). \quad (81)$$

The impermeability of the top and bottom surfaces tells us $p_z = 0$ on $z = 0, d$. Evidently this condition is satisfied identically at leading order by (80). Therefore we have to consider higher-order terms to deduce the leading-order boundary conditions

$$(\lambda + \mu)U_{xz} + (\lambda + 2\mu)W_{zz} = 0 \quad \text{on } z = 0, d. \quad (82)$$

Substituting for U from (81) we can now solve (78, 82) as a boundary-value problem for W_z . However, when we look for periodic solutions proportional to $e^{i\omega t}$, it is not necessary to solve for W explicitly, since we can integrate (78) directly with respect to z and find

$$i\omega \int_0^d U_x dz + i\omega [W]_0^d = D [U_{xz} + W_{zz}]_0^d. \quad (83)$$

Now W is given on the top and bottom surfaces by (68, 70), $W_z z$ by (82) and U by (81), so that (83) reduces to

$$i\omega \left(\frac{d^3 p_{xx}}{12\mu} + h \right) = -\frac{dD p_{xx}}{\lambda + 2\mu} = -\frac{d\alpha_0 k(\alpha_0) p_{xx}}{\eta}. \quad (84)$$

For $p(x)$ we have the symmetry condition $p_x = 0$ at $x = 0$ and $p = 0$ at the edge $x = l$ (neglecting any pressure drop across the unsqueezed portion in $x > l$). Thus (84) gives

$$\frac{i\omega}{2} (l^2 - x^2) = \left(\frac{d\alpha_0 k(\alpha_0)}{\eta} + \frac{i\omega d^3}{12\mu} \right) p. \quad (85)$$

Finally, in the lubrication approximation the force F is given to lowest order by

$$F = 2 \int_0^l p dx \quad (86)$$

and thus

$$\frac{2i\omega h l^3}{3} = \left(\frac{d\alpha_0 k(\alpha_0)}{\eta} + \frac{i\omega d^3}{12\mu} \right) F, \quad (87)$$

so that the effective complex modulus is

$$G = \frac{2i\omega l^3 \eta}{3d\alpha_0 k(\alpha_0)} \left(1 + \frac{i\omega d^2 \eta}{12\mu\alpha_0 k(\alpha_0)} \right)^{-1}. \quad (88)$$

Thus we have succeeded in obtaining a lumped-parameter model for the squeezing problem. Indeed, (88) takes exactly the same form as the linear lumped-parameter model (25) considered previously (with $d = 0$). Thus in the asymptotic limit employed in this section, the effects of elasticity and porous-medium flow combine to make the material behave exactly like a linear Maxwell fluid. The advantage of the approach adopted here is that we can associate the parameters in (88) with real physical properties of the system such as porosity, viscosity, Youngs modulus, *etc.*

The expression (88) has a number of interesting properties. Notice that the bulk modulus λ does not appear so that, although the details of the spatial variations in $\tilde{\alpha}$, W , *etc.* depend on λ , the response of the system as a whole does not. This is a consequence of the lubrication limit, and can be explained physically as follows. When the sponge is compressed, liquid is squeezed out horizontally by pure kinematics. The lateral flow of liquid is resisted by *shear stress* in the solid matrix, and it is this shear stress which is responsible for the pressure build-up, as described by (79).

We also note that an important dimensionless parameter sits in the denominator of (88), namely

$$\mathcal{D} = \frac{i\omega d^2 \eta}{12\mu\alpha_0 k(\alpha_0)}, \quad (89)$$

which is an effective Deborah number. As $\mathcal{D} \rightarrow \infty$, the material becomes elastic, with

$$G \sim \frac{8\mu l^2}{d^3},$$

while as $\mathcal{D} \rightarrow 0$, we find

$$G \sim \frac{2i\omega l^3 \eta}{3d\alpha_0 k(\alpha_0)},$$

i.e. a purely viscous response.

4 Conclusions

The work of this report falls broadly into two parts. First we analysed experimental data generated at the study group in an attempt to find good robust indicators of a particular sample's material properties. Encouragingly we found two scalar properties which appear, at least with the limited data considered so far, to vary significantly from one sample to another, and to be readily measurable. It should be straightforward to check whether they are at all correlated with fish freshness.

We went on to present some possible mathematical models for the testing process. We considered linear elasticity and viscoelasticity as well as deformable porous medium models, in a variety of geometries. None of these models comes close to capturing all the complications of a real fish. However they should aid understanding of the importance of various physical effects such as elasticity and porosity.

We conclude by suggesting further experiments which could be carried out in the future.

4.1 Proposed future experiments

1. The proposed system is based on the idea that the constitutive properties of fish (*i.e.* elastic and viscous moduli) can be used to measure its freshness. Before proceeding any further with the project, it should be verified that the properties which could be measured by this kind of machine really do vary with age of fish. Thus samples of different species, age and taken from different parts of the fish, should be tested in a professional rheometer over a wide range of frequencies. This would determine (*i*)

whether rheological properties are at all correlated with fish age, and if so (*ii*) which are the best indicators of freshness and (*iii*) what frequency range a testing machine should be designed to measure.

2. In any such machine, and in future experiments, it would make more sense to impose a sinusoidal force (or displacement) rather than the sawtooth forcing used at present. This would both simplify any mathematical modelling and tie in with more traditional rheometry.
3. The measurement of the speed and attenuation of sound waves might a good way to determine the mechanical properties. Note that this would only be worthwhile if the rheological tests suggested in **1.** above show that such properties are well correlated with freshness. Note also that the limit of interest here is the opposite of that used in acoustic microscopy: we do not wish to resolve the details of the skeleton *etc.* of the fish but rather to obtain some locally averaged properties.

Acknowledgements

We are grateful to Paul Nesvadba and David Simmonds for bringing this stimulating problem to the Study Group. Other people who worked on the problem include Paul Bolchover, John Byatt-Smith, Warrick Cooke, Jeff Dewynne, Gail Duursma, Paul Everall, Alistair Fitt, Jens Gravesen, Julie Guneratne, John Hinch, Peter Howell, Sam Howison, John King, Andrew Lacey, Raphael Morones Escobar, John Ockendon, David Parker, Colin Please, Domingo Salazar-Gonzalez, Gareth Shaw, Nick Stokes, Graham Veitch. Apologies for any omissions.

The report was written by Peter Howell and Paul Bolchover.

References

- BIOT, M.A., 1955 Theory of elasticity and consolidation for a porous anisotropic solid, *J. Appl. Phys.* **26**, 182–185.
- CALLADINE, C. R., 1985 *Plasticity for Engineers*, Ellis Horwood.
- ENGLAND, A. H., 1971 *Complex variable methods in elasticity*, Wiley.
- SOMMER, J. L. & MORTENSEN, A., 1996 Forced unidirectional infiltration of deformable porous media, *J. Fluid Mech.* **311**, 193–217.
- SPENCE, D. A., 1968 Self similar solutions to adhesive contact problems with incremental loading, *Proc. Roy. Soc. A.* **305**, 55–80.

